Acta Materialia 138 (2017) 1–9

Contents lists available at ScienceDirect

Acta Materialia

journal homepage: www.elsevier.com/locate/actamat

Full length article

High temperature brittle film adhesion measured from annealing-induced circular blisters

Tao Guo [a], Jianying He [b], Xiaolu Pang [c, *], Alex A. Volinsky [d], Yanjing Su [a], Lijie Qiao [a, **]

[a] Corrosion and Protection Center, Key Laboratory for Environmental Fracture (MOE), University of Science and Technology Beijing, Beijing 100083, China
[b] NTNU Nanomechanical Lab, Department of Structural Engineering, Norwegian University of Science and Technology (NTNU), Trondheim 7491, Norway
[c] Department of Materials Physics and Chemistry, University of Science and Technology Beijing, Beijing 100083, China
[d] Department of Mechanical Engineering, University of South Florida, Tampa, FL 33620, USA

ARTICLE INFO

Article history:
Received 5 April 2017
Received in revised form
28 May 2017
Accepted 11 July 2017
Available online 12 July 2017

Keywords:
High temperature adhesion
Circular blisters
Dislocation shielding
Phase transformation
Interfacial embrittlement

ABSTRACT

Testing high temperature brittle film adhesion is necessary for understanding interfacial failure at elevated temperatures. However, current brittle film adhesion measurement methods are limited to room temperature. Experimental techniques to characterize high temperature brittle film adhesion are lacking, and temperature effects on brittle film adhesion remain poorly understood. Here, a simple, yet reliable method is developed to measure the adhesion of TiN films on Si substrates with native SiO_2 oxide layer from 300 °C to 500 °C, based on circular blisters induced by annealing. The circular blister size was proven to remain the same after cooling down to room temperature, based on *in situ* observations. Experimental results show that film adhesion energy gradually increases and then drops with annealing temperature. Thermally activated dislocation glide promotes easier nucleation of dislocations in Si substrate near the interface. This in turn increases dislocation shielding effects on the interfacial crack tip during its dynamic propagation, resulting in the initially increased adhesion with temperature. Plastic deformation of TiN film is not considered because the combination of the small grain size of less than 10 nm and the amorphous/nanocrystalline structure limits dislocation emission and grain sliding. Local phase film transformation from amorphous to nanocrystalline at the TiN/SiO_2 interface was demonstrated by high resolution transmission electron microscopy, causing adhesion reduction due to interfacial embrittlement and contact mismatch at 500 °C. In addition, the drop in adhesion induces circular blisters' transition from axisymmetric to non-axisymmetric.

1. Introduction

Brittle coatings are used to improve underlying substrates' mechanical and functional properties at elevated temperatures. Examples include protection coatings to prevent high temperature oxidation [1], diffusion barrier layer to inhibit interdiffusion between metal film and the substrate at high temperature [2], and thermal barrier coatings to improve operating temperature of turbine blades [3]. However, high temperature can induce coating compressive stress [1,4], increase interfacial roughness [5], or introduce chemical impurities [6], which promote interfacial delamination [7–9] and tremendously limit brittle coating applications at elevated temperatures. For reliable coating/substrate design, testing adhesion at elevated temperatures, along with understanding the factors affecting adhesion, are not only scientifically, but also practically necessary for engineering applications.

In the past decades, lots of methods have been proposed to determine brittle film adhesion qualitatively and quantitatively. Qualitative methods include pull off and peel tests, also known as tap tests [10]. To measure the adhesion energy quantitatively, five typical methods have been used, including scratch [11,12], four-point bending [13,14], stressed overlayers [15], hydrogen induced buckling [16,17] and nanoindentation [18,19] tests. These methods have been successfully used to study adhesion of brittle films at room temperature. However, measuring thin film adhesion at elevated temperatures has been challenging due to the testing difficulties, including sample preparation, accurate temperature measurements, controlling environment to prevent sample oxidation, and so on. As a result, only a few studies investigated the thin

* Corresponding author.
** Corresponding author.
E-mail addresses: pangxl@mater.ustb.edu.cn (X. Pang), lqiao@ustb.edu.cn (L. Qiao).

http://dx.doi.org/10.1016/j.actamat.2017.07.026
1359-6454/

films' adhesion at elevated temperatures, but have been limited to temperatures below 130 °C using nanoindentation methods [20,21]. Adhesion of brittle films at elevated temperatures remains an unexplored area.

A large amount of work dealing with film adhesion at room temperature has suggested that many factors affect adhesion, including residual stress [22,23], film grain size [18,20,21], film/substrate interfacial structure and composition [24], and plastic energy dissipation in the film and/or the substrate [11,18,25–27]. Of particular note, all of these factors are inevitably affected by temperature. For example, temperature remarkably increases compressive stress in β-NiAl [1] and TiN [4] films on Si substrates due to the difference in thermal expansion coefficients. At elevated temperatures, thermally activated dislocation glide, grain boundary diffusion creep, and dislocation-based creep are more pronounced [28,29], contributing to an enhanced toughness, in particular near the brittle-to-ductile transition temperature [30]. Some studies have demonstrated that interdiffusion [31] and reactions between the film and the substrate, or adhesion layer at elevated temperature, can lead to the formation of new phases [24]. These studies imply that the high temperature film adhesion energy differs substantially from the room temperature values. Therefore, a new simple method to measure brittle film adhesion at elevated temperature is required.

If the film has a larger thermal expansion coefficient than the substrate, large compressive stress will arise with increasing temperature [1,4], inducing some interesting buckling morphology, including straight-sided blisters [9], circular blisters [32,33], and telephone cord buckles [8,15,34]. These buckling patterns with well-defined shapes have been utilized to evaluate mechanical parameters, such as the stress level [35] and adhesion energy [12,15,36,37] of brittle films at room temperature, by employing the elastic buckling model proposed by Hutchinson and Suo [38]. Similarly, buckling can also be used to characterize brittle film adhesion at high temperature and its dependence on temperature.

In this paper, we present a simple, but reliable method based on annealing-induced circular blisters' formation to determine the adhesion of TiN films on Si substrates with native SiO_2 oxide at high temperatures. Confocal laser scanning microscope (CLSM) was used to measure the circular blister dimensions (height and diameter). The dependence of film adhesion on temperature has been studied, and the corresponding mechanisms have been proposed.

2. Experimental procedure

TiN films were deposited on 20 mm × 20 mm (111) Si substrates with native SiO_2 oxide using reactive RF-pulsed magnetron sputtering at 300 °C. The substrates were moved in front of the titanium target (99.99% pure) with a diameter of 76 mm. In order to weaken the interface, all substrates were not subjected to Ar plasma cleaning [39], thus, buckling was more likely to appear during film annealing. In the magnetron sputtering system used for film deposition, the base pressure was 2×10^{-3} Pa, the target power was 250 W, and the Ar working gas pressure was 0.3 Pa. Nitrogen gas flow during deposition was 0.9 cm^3/min, while argon flow was 30 cm^3/min. The nominal film thickness was about 600 nm, measured by CLSM (LEXTOLS4000, Olympus, Japan).

The change of the film surface topography with temperature was observed *in situ* by ultra-high temperature CLSM (VL2000DX-SVF17SP, Lasertec), which used infrared heating. The chamber was first pumped to 10^{-2} Pa, and then vented with Ar (≥99.99% pure) for 30 min before heating to prevent film oxidation. Due to larger thermal expansion coefficient of TiN film compared with the Si substrate [4], biaxial compressive stress in the film was generated during heating. Once the thermal stress approached the film critical debonding stress, circular crack formed at the TiN/SiO_2 interface, because the adhesion between the native SiO_2 oxide layer and Si substrate is much stronger than between the sputtered layer and SiO_2 [18,23,40,41]. The compressive stress would load the edge of the interface crack between the film and the substrate, causing the blister to spread, as seen in Fig. 1b–d. During annealing, the blister's diameter grew initially and then arrested, as seen in Fig. 1d–g. During cooling, the size of the blister remained the same due to the decrease in the biaxial compressive stress, i.e. the decrease in driving force for the blister propagation, as seen in Fig. 1g–i. Unfortunately, the ultra-high temperature CLSM (VL2000DX-SVF17SP, Lasertec) was unable to observe the three-dimensional topography, i.e. the height of the blisters. According to the previous *in situ* observations of the straight-sided blister growth [9], the height of the blister is related to its width, i.e. the height won't change if the width is kept the same. Therefore, the stabilized dimensions of the blisters at elevated temperature can be replaced by those at room temperature, and then the film adhesion at elevated temperature can be measured.

The original as-deposited sample was cut into smaller pieces, about 4 mm × 4 mm in size, and randomly divided into eight sets. Five sets of samples were placed into quartz tubes with 10^{-5} Pa pressure to prevent samples oxidation. Samples were annealed at various temperatures ranging from 300 °C to 500 °C, with a 50 °C interval, 5 °C/min heating rate and kept for 2 min at set temperature to stabilize the blisters morphology, and then naturally cooled in the furnace to room temperature. The blister topography of each sample after annealing was obtained at room temperature using CLSM (LEXTOLS4000, Olympus). More than 100 blisters were measured for each temperature to obtain average adhesion values.

X-ray diffraction (XRD) experiments were carried out in the 10°–90° 2θ range with Cu Kα radiation (TTRIII, Rigaku). The interfacial structure between the film and the substrate was observed in cross-section with high resolution transmission electron microscopy (HRTEM, Tecnai G2 F20 FEI). Young's modulus and hardness of the films were measured by nanoindentation using Berkovich tip with an effective radius of 150 nm (TI900, Hysitron). The fracture toughness of annealed TiN films was measured by the indentation method [42], using a Vickers hardness tester (HV-1000, ALEC), with a load of 0.98 N.

3. Experimental results

3.1. Microstructure of TiN films at elevated temperature

Fig. 2 shows XRD patterns of TiN films on Si substrates in the as-deposited and annealed states obtained under the same XRD measurement conditions. An obvious increase in XRD intensity is observed in the film annealed at 500 °C compared to the as-deposited state, indicating higher degree of film crystallization with annealing [43,44]. Another observation is that no detectable film oxidation occurred during annealing, since only TiN diffraction reflections are present in the XRD patterns.

Fig. 3 shows interfacial HRTEM and the corresponding selected area electron diffraction (SAED) patterns. Fig. 3a reveals that the as-deposited TiN film consists of a purely amorphous layer, about 15 nm thick, followed by a layer with amorphous/nanocrystalline structure. The presence of thin amorphous layer near the interface is also observed in other sputter-deposited brittle films [45,46], which is attributed to rapid quenching of atoms as they arrive onto the substrate [47,48]. However, sputter deposition will heat the substrate, resulting in increased surface mobility of the film constituents, which favors the film growth with higher degree of crystallization further away from the interface [46,48]. No obvious crystallization of the amorphous layer is observed after 300 °C

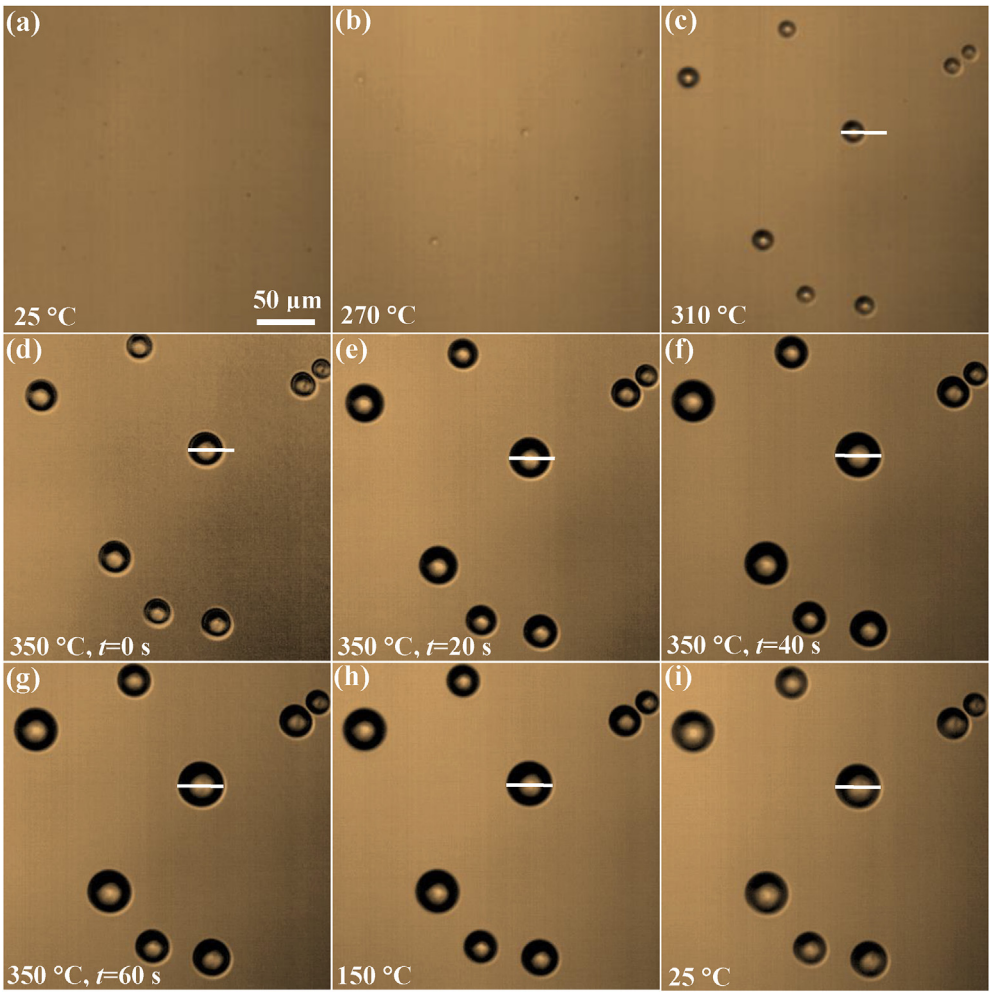

Fig. 1. The *in situ* observation of blister nucleation and propagation during annealing: (a)–(d) Heat to 350 °C at 30 °C/min rate; (d)–(g) Hold at 350 °C for 60 s; (g)–(i) Cool to room temperature at 30 °C/min rate. The white bars across the blisters in all images have the same length for illustration purposes. All figures have the same scale.

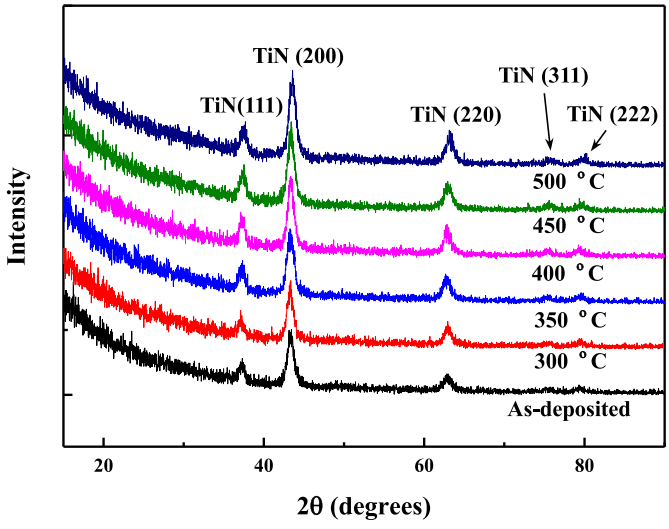

Fig. 2. XRD results of as-deposited and annealed TiN films.

annealing, according to the interfacial HRTEM and the corresponding fast Fourier transform (FFT) of the inset in Fig. 3b. With further increase of annealing temperature to 400 °C (higher than the 300 °C deposition temperature), crystallization appears in the amorphous layer, while the film near the interface remains amorphous, as clearly seen in Fig. 3c. Of particular interest, as the annealing temperature increases to 500 °C, TiN nanocrystals form at the TiN/SiO_2 interface, as seen in Fig. 3d. A higher degree of film crystallization at 500 °C than in the as-deposited state is also observed, by comparing the SAED patterns in Fig. 3a and d, which is consistent with the enhancement of diffraction reflections intensity in XRD patterns in Fig. 2. Fig. 3e shows that the 500 °C annealed film contains nanocrystals with grain size of less than 10 nm embedded in the amorphous matrix. Similar structure is also observed in as-deposited and other annealed TiN films (not shown in the paper). In addition, no interdiffusion between the film and the substrate is observed. This agrees with previous studies of the thermal stability of TiN film on Si substrates [49]. This result also suggests that the diffusivity of Si through dense TiN is extremely limited, even after annealing for 20 h at 700 °C.

3.2. Blister propagation with temperature

As mentioned in the experimental section, circular blisters tend to form and propagate at elevated temperature, as seen in Fig. 4a and b. Higher annealing temperature induces larger compressive stress in the film, so the blisters in Fig. 4c either keep propagating or spall off from the substrate due to cracks kinking out of the

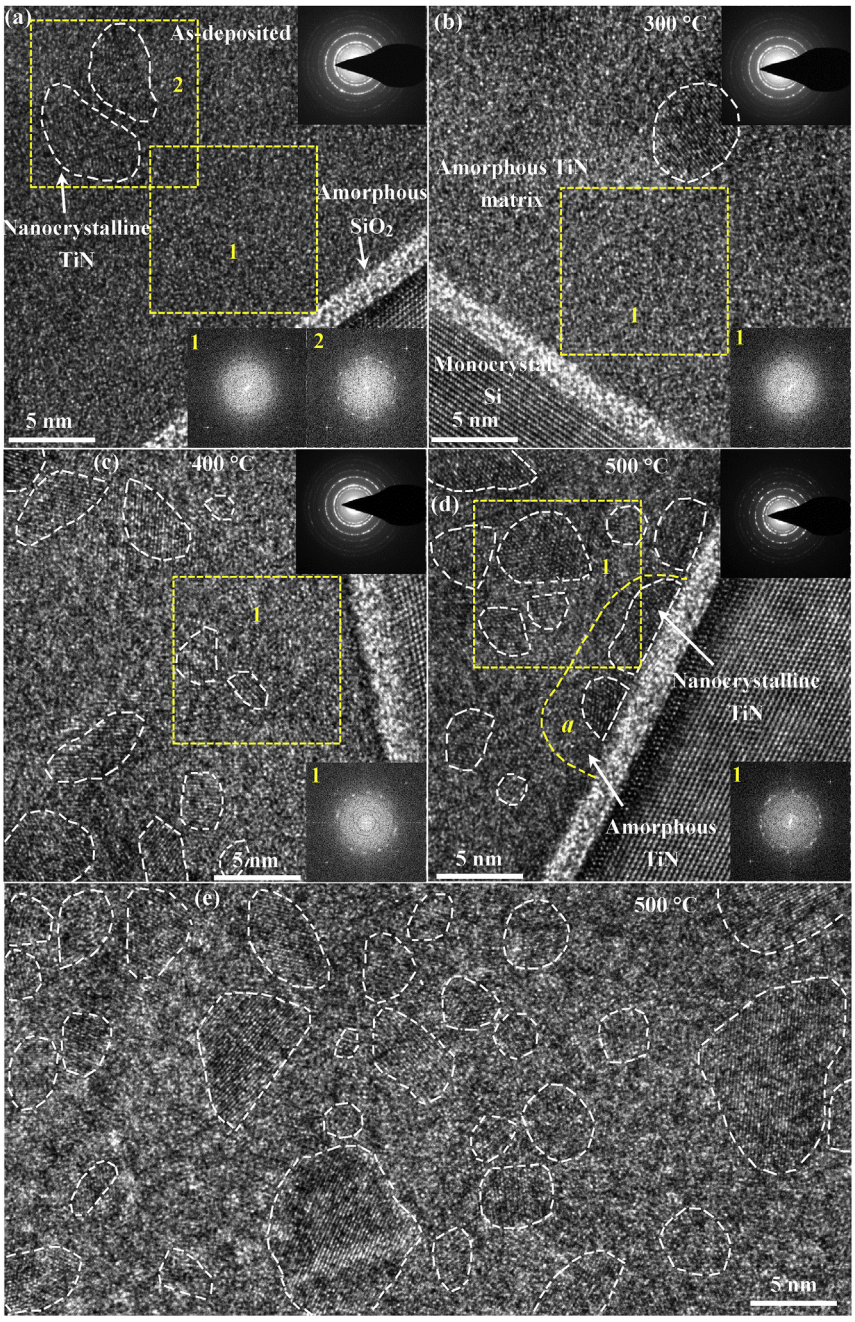

Fig. 3. Representative HRTEM images of the interface in the as-deposited and annealed states: (a) As-deposited; (b) Annealed at 300 °C; (c) Annealed at 400 °C; and (d) Annealed at 500 °C. Figures insets in the upper right corner of (a)–(d) are SAED patterns of the film near the interface with a diameter about 150 nm (the smallest area that the TEM can probe). Figures insets in the bottom right corner of (a)–(d) are the FFT images of the film near the interface marked by the yellow dashed squares on the HRTEM image. The selected area *a* in (d) near the interface is comprised of the amorphous and nanocrystal TiN. (e) Representative HRTEM image of the film annealed at 500 °C. Native amorphous SiO2 oxide layer on the single crystal Si is about 1.6 nm thick. TiN nanocrystals are circled by the white dashed lines. (For interpretation of the references to colour in this figure legend, the reader is referred to the web version of this article.)

interface into the film [38,50]. The blisters remain circular in shape until a critical size is reached, where they start to lose their circular symmetry, forming non-symmetric perturbations, as marked by the blue arrows in Fig. 4d. Similar phenomenon was also observed in the mica/aluminum system [33], attributed to the increasing value of the film residual stress to critical buckling stress ratio, σ_r/σ_c, during blister propagation. As the annealing temperature approaches 500 °C, all large blisters lose their circular symmetry, and some small blisters exhibit non-axisymmetric propagation, marked by blue arrows in Fig. 4e. Only these blisters with much smaller diameters remain circular, as marked by green dashed arrows in Fig. 4e.

3.3. Temperature-dependent adhesion of TiN films

Most of the mechanical tests measure film adhesion at room temperature by delaminating thin films from the substrates [19]. During debonding from the substrate, the thin film and/or the substrate usually experience plastic deformation, giving an apparent work of adhesion, often termed as the practical work of

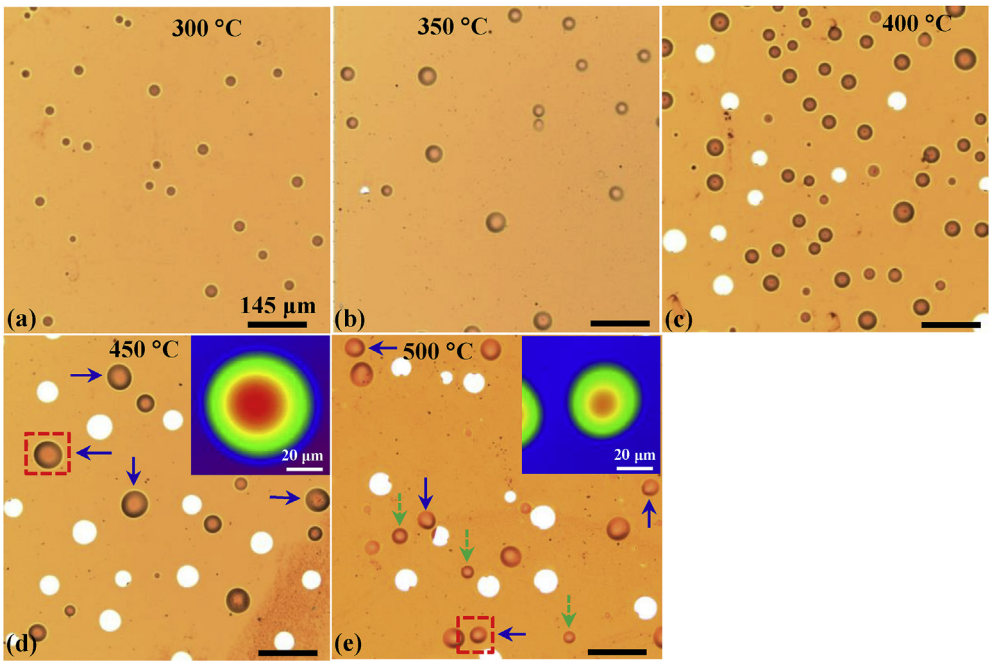

Fig. 4. Representative optical microscopy images of TiN films after annealing at: (a) 300 °C; (b) 350 °C; (c) 400 °C; (d) 450 °C; and (e) 500 °C. The white zones are substrates where film spalled off. Images (a)–(e) have the same scale. Figures insets are two-dimensional CLSM images of the selected blisters marked by the red dashed squares. (For interpretation of the references to colour in this figure legend, the reader is referred to the web version of this article.)

adhesion. It can be defined as the work of interfacial separation plus the energy dissipation in the film and the substrate [19]. In the elastic buckling model proposed by Hutchinson and Suo [38] for adhesion energy, the blister is treated as a clamped circular elastic plate. The plate has a radius a, height δ, and film thickness h, as shown schematically in Fig. 5. In Fig. 5 the unbuckled film is subjected to biaxial compressive in-plane stress and h is much smaller than a. The adhesion energy can be calculated using the critical buckling stress, σ_c, and the residual stress, or the driving stress, σ_r [38]:

$$\sigma_c = 1.2235\frac{E}{1-\nu^2}\left(\frac{h}{a}\right)^2 \tag{1}$$

$$\sigma_r = \sigma_c\left[1 + c_1\left(\frac{\delta}{h}\right)^2\right] \tag{2}$$

where $c_1 = 0.2473(1+\nu) + 0.2231(1-\nu^2)$ [38], and E and ν are the film elastic modulus and Poisson's ratio, respectively. The asymptotic result for the adhesion energy (Γ_a) is [38]:

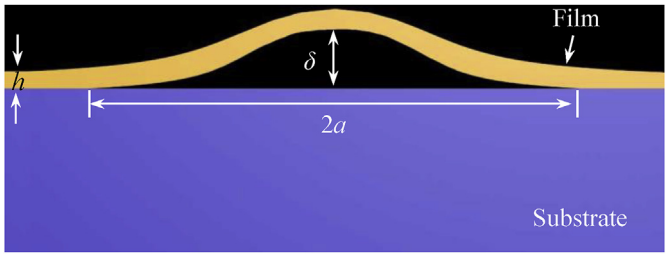

Fig. 5. Cross-sectional schematic of a circular blister.

$$\frac{\Gamma_a}{G_0} = c_2\left[1 - \left(\frac{\sigma_c}{\sigma_r}\right)^2\right] \tag{3}$$

where $c_2 = [1 + 0.9021(1-\nu)]^{-1}$ [38], and G_0 is the strain energy release rate per unit area stored in the unbuckled film [38]:

$$G_0 = (1-\nu)h\sigma_r^2/E \tag{4}$$

By inserting Eqs. (1), (2) and (4) into Eq. (3) and using $\nu = 0.25$ [51], the adhesion energy can be obtained as:

$$\Gamma_a = 0.72hE\left(\frac{h}{a}\right)^4\left[0.27\left(\frac{\delta}{h}\right)^4 + \left(\frac{\delta}{h}\right)^2\right] \tag{5}$$

Eq. (5) is only valid for stress ratios (σ_r/σ_c) of less than 2 [38], i.e. the height of the blisters should be less than 0.83 μm, according to Eq. (2), with a film thickness of 0.6 μm in our case. When σ_r/σ_c is larger than 2, numerical analysis results must be used to calculate the film adhesion energy (Γ_n):

$$\Gamma_n = \chi\Gamma_0 \tag{6}$$

The parameter χ can be obtained from Fig. 64a in Ref. [38], which presents the Γ_n/G_0 variation with σ_r/σ_c, based on the numerical analysis results.

As indicated in Eq. (5), the calculated adhesion energy is affected by the elastic modulus, which increases with annealing temperature, as shown in Table 1. Examples include amorphous Ni-P [52] and Cr_2O_3 [53] coatings, whose elastic modulus increases with temperature because crystalline materials have higher elastic modulus than their amorphous counterparts. However, to the best of our knowledge, there is no experimental data of the elastic modulus for polycrystalline TiN films at elevated temperatures. Previous experimental studies of polycrystalline ceramics' elastic modulus dependence on temperature [54–56], including ZrB_2,

Table 1
Mechanical properties of TiN films annealed at different temperatures.

	300 °C	350 °C	400 °C	450 °C	500 °C
Hardness H (GPa)	19.5 ± 0.5	20.3 ± 0.4	21.9 ± 0.8	22.9 ± 1.2	24.4 ± 1.1
Elastic modulus E_{RT} (GPa)	251.2 ± 3.2	255.8 ± 4.3	267.8 ± 3.9	273.4 ± 4.5	281.2 ± 5.6
Fracture toughness K_{IC} (MPa·m$^{1/2}$)	0.68 ± 0.02	0.66 ± 0.04	0.58 ± 0.07	0.54 ± 0.02	0.49 ± 0.03
Elastic modulus at elevated temperatures estimated from MD simulations, E(T) (GPa) [58]	0.96 E_{RT} 241.2	0.952 E_{RT} 243.5	0.944 E_{RT} 252.8	0.937 E_{RT} 256.2	0.93 E_{RT} 261.5

E_{RT}: Film elastic modulus after annealing, measured at room temperature.

Al_2O_3, MgO, SiN, PbTe, etc., suggest that the elastic modulus of brittle polycrystalline materials decreases gradually at first, and then drops more rapidly at much higher temperatures. The initial decrease can be described by a linear relationship [57]:

$$E(T) = E_{RT}[1 - b(T - T_R)] \quad (7)$$

where E_{RT} is the room temperature elastic modulus, b is a fitting parameter and T_R is room temperature. The subsequent drop is attributed to grain boundary softening and sliding [57]. However, as seen in Fig. 3e, the film in the present study has an amorphous/nanocrystalline structure without any grain boundaries. As a consequence, the elastic modulus of TiN films at elevated temperatures can be obtained by Eq. (7), by using the fitting parameter b from molecular dynamics simulations of the polycrystalline TiN elastic constants dependence on temperature [58], as listed in Table 1.

As assumed in the Hutchinson and Suo model [38], the approach of using Eqs. (5) and (6) is only valid if the blister has a symmetric cross-section and deforms elastically. In the present study, plastic processes in TiN films are ignored, due to the combination of small grain size and amorphous/nanocrystalline structure, which will be discussed in section 4.1. Fig. 6 is an example showing representative CLSM images of an axisymmetric circular blister of TiN film annealed at 450 °C. The profile along the radial direction is measured to obtain the height (δ) and diameter of the blister (a), as indicated in Fig. 6b and c. These non-axisymmetric blisters have been ignored in adhesion measurements reported in this paper. According to Eqs. (5) and (6), the high temperature TiN film adhesion energy is obtained, which increases gradually with annealing temperature, and then drops, as seen in Fig. 7. The reduction of adhesion can be used to understand the non-axisymmetric propagation of smaller blisters in Fig. 4e. As mentioned before, the increasing value of the film residual stress to critical buckling stress ratio, σ_r/σ_c (i.e. the increasing blister size according to Eq. (2)), induces non-axisymmetric blister propagation [33]. In addition, the buckling process is also affected by the film/substrate interfacial adhesion. For the same film thickness, the weaker the interfacial adhesion, the lower the critical buckling stress [59,60]. As a consequence, as the adhesion drops, a smaller blister size is needed to obtain the critical stress ratio for the circular blister starting to propagate non-symmetrically, compared to the film with better adhesion. Under the critical size, the blisters still remain circular symmetric, as marked by the green dashed arrows in Fig. 4e.

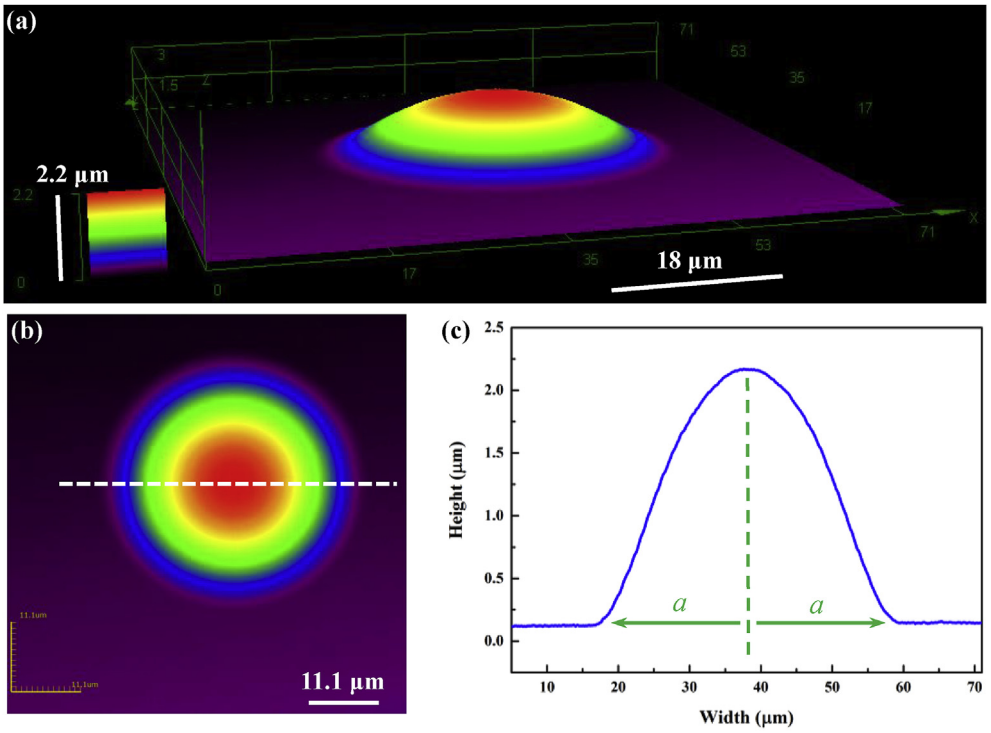

Fig. 6. The CLSM images of TiN film annealed at 450 °C: (a) Three-dimensional topography; (b) Two-dimensional morphology and (c) The profile of the selected blister in (b) along the white dashed line, showing the blister circular symmetry.

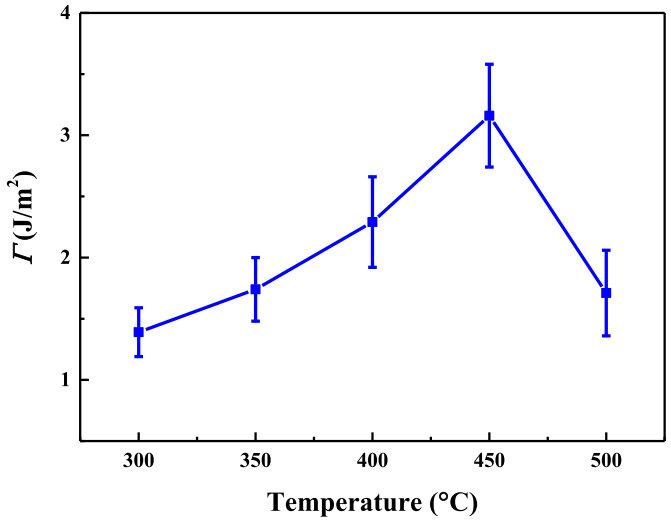

Fig. 7. Measured adhesion at elevated temperatures according to Eqs. (5) and (6). The error bars indicate the standard deviations from more than 100 circular blisters measured on each sample set.

4. Discussion

4.1. Amorphous/nanocrystalline structure effect on TiN film plasticity

In the present study, TiN films have a structure comprising of nanocrystals with less than 10 nm size embedded in amorphous matrix, as seen in Fig. 3. A number of research reports [61–65] focused on super-hard coatings, have suggested that nanocrystalline grains (several nanometers) imbedded in an amorphous matrix in the two-phase nanocomposite films enhance the film hardness or strength. It has been demonstrated that the nanocrystals with less than 10 nm size cannot accommodate any dislocation multiplication sources, leading to nanocrystals being free of dislocations [64,65]. Even if some dislocations may be emitted within these nanocrystals due to the increased applied stress or experimental temperature, they could not slip through the amorphous phase, because randomly oriented nanocrystals inserted within the amorphous matrix provide a better coherence at the interface than purely polycrystalline materials [64]. The high cohesive strength between the nanocrystals and the amorphous matrix also hinders grain sliding [64], which contributes to the plastic deformation in polycrystals [28]. As a consequence, the plastic energy dissipation in the present TiN films is extremely limited, then the deformation of films can be regarded as elastic, even at elevated temperatures. This embrittlement phenomenon would be more pronounced with better film crystallization as annealing temperature rises [52,53]. A similar phenomenon of K_{IC} decrease is also observed in the present study, as seen in Table 1.

4.2. Temperature effects on brittle film adhesion

Previous explanations [18,20,21,23,66] for the enhancement in the measured adhesion energy at room temperature due to the increasing plastic energy dissipation both in the film and the substrate, are mainly based on the dislocation free zone (DFZ) model, proposed by Gerberich et al. [20]. In the model, the yield strength (determined by the grain size) both of the film and the substrate is the key factor that contributes to the plastic energy dissipation. However, this model is unsuitable for the present study, due to the extremely limited plastic energy dissipation in the TiN films and single crystal Si substrate. As seen in Fig. 4, film buckling and interface cracking are both involved in the propagation of blisters with temperature. At a given applied compressive stress, the buckling behavior of the film is determined by the elastic modulus [67], which does not change significantly in the present experimental temperature range. The interfacial cracking behavior is controlled by the plastic deformation (both in the film and the substrate) in front of the crack tip [68]. Here, we attribute the increase in adhesion with temperature to the increasing plastic energy dissipation in the substrate in front of the dynamic interfacial crack during propagation with rising temperature, known as the dislocation shielding effect [68–72].

Dislocations can be emitted near the indentation or crack tip in single crystal Si under external stress at room temperature [73–75]. The emission of dislocations near the crack tip can be described by the Rice and Thomson model [76]. The force, τ_i on the i_{th} dislocation of per unit length is given as [76]:

$$F_i = \frac{K_{app}}{r_i^{1/2}} f(\theta) - \frac{Gb}{4\pi r_i} - \tau_f b - \frac{Gb}{2\pi} \sum_{\substack{i=1 \\ j=1}}^{N} \frac{\sqrt{r_i/r_j}}{r_i - r_j} \tag{8}$$

where K_{app} is the applied stress intensity factor, r_i is the distance to the dislocation from the tip of the crack, θ is the angle between the slip plane and the crack plane, G is the shear modulus, τ_f is lattice friction for dislocation to move, b is the Burgers vector, and N is the number of dislocations in front of the crack tip. In the present study, K_{app} is related to the tensile stress near the crack tip imposed by the film during heating, due to the difference in thermal expansion coefficients, $\sigma = (\alpha_f - \alpha_s)(T_r - T_0)E_f/(1 - \nu_f)$, where α is the thermal expansion coefficient of film and substrate, respectively. In Eq. (8), the first term is related to the crack-tip stress field, and the second term is the image force induced by the crack on the dislocation at a distance r_i. The third term is the frictional force for the dislocation to move, and the fourth term describes the image force of all other dislocations on the one dislocation, $i \neq j$. Dislocations will be produced at the dislocation source if the total force is positive, and move away along the slip plane to form a one-dimensional array on a single slip plane, as shown schematically in Fig. 8. The existence of the amorphous thin native SiO_2 layer can inhibit dislocations escaping from the Si substrate. Then they will pile up near the SiO_2/Si interface, which results in two competing

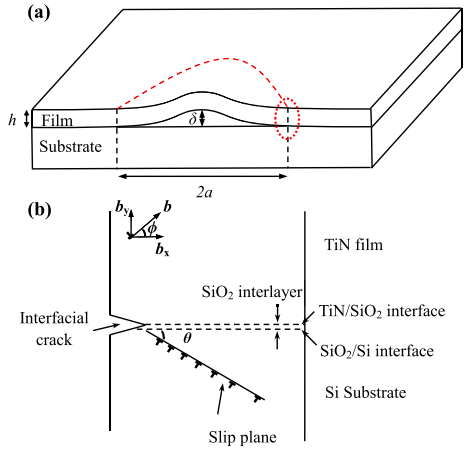

Fig. 8. (a) Cross-sectional schematic of the circular blister debonding from the substrate. (b) The geometry of dislocation, crack and film-substrate interface. Edge dislocations pile up along the slip plane in the substrate region near the interfacial crack tip.

effects. One is producing a back stress to hinder further dislocation emission from dislocation sources in Si, according to Eq. (8). The other is blunting of the interfacial crack, leading to the reduced stress intensity at the crack tip [68,70]:

$$K_{tip}(t) = K_{app}(t) - K_{dis}(t) = \dot{K}_{app}t - \frac{Gb}{2\pi(1-\nu)}\sum_{i=1}^{N(t)} r_i(t)^{-1/2} \tag{9}$$

Here, $\dot{K}_{app}$ is the applied stress intensity factor rate, G is the shear modulus, b is the Burgers vector, $r_i(t)$ is the distance of each dislocation to the crack tip, and $N(t)$ is the number of dislocations in front of the crack tip.

Plastic deformation in single crystal Si will be much more remarkable at elevated temperatures [30,77,78], which is mainly controlled by thermally activated dislocation glide [30]. The kinetic process of dislocation motion obeys an empirical relation of the dislocation velocity [79]:

$$v = v_0\left(\frac{\tau}{\tau_0}\right)^m exp\left(-\frac{E_m}{kT}\right) \tag{10}$$

where v_0 is the material specific reference dislocation velocity, τ_0 is the reference shear stress, and m is the stress exponent. τ is the shear stress on the dislocation, E_m is the activation energy for dislocation glide, k is the Boltzmann constant, and T is the absolute temperature. It has been established that the number of dislocations near the crack tip depends on dislocations' mobility, i.e. how easily the emitted dislocations move away from the crack tip [30]. As indicated by Eq. (10), increasing temperature allows faster mobility of dislocations, leading to easier nucleation of dislocations, because of the reduction in back stress [77,80]. With more dislocations emitted in the substrate near the crack tip, the dislocation shielding effect at a given K_{app} is promoted, leading to the reduction of K_{tip}, then the fracture of interface is delayed. If the interface cracking is restricted, the film buckling will be promoted to respond to the thermal compressive stress, resulting in the increased measured adhesion energy with temperature ranging from 300 °C to 450 °C.

The cracking of the interface is mainly controlled by the interfacial structure and components, i.e. local mechanical properties of the film and the substrate near the interface [24,81]. As seen in Fig. 3d, the phase transformation from amorphous to nanocrystalline in the film at the TiN/SiO_2 interface has two synergistic effects on adhesion. One is that the formation of amorphous/nanocrystalline structure in a local area at the interface, such as highlighted area *a*, significantly contributes to the interface embrittlement. The other one is that the crystallization of film increases the misfit of interface compared with the previous amorphous state. Similar behavior is also observed in the Ti/PI system, where the interfacial adhesion reduces drastically from 4.7 J/m^2 to 1.4 J/m^2 due to the interfacial phase transformation from amorphous to nanocrystalline after annealing [81]. The combination of these two effects decreases the adhesion, and the decrease couldn't be compensated by the increasing plastic energy dissipation in the Si substrate, leading to the drop in the measured interfacial adhesion energy as the temperature rises to 500 °C.

5. Conclusions

High temperature adhesion energy of TiN films on Si substrates was successfully determined from the circular blisters induced by annealing. TiN films have a structure comprising of nanocrystals with less than 10 nm size embedded in amorphous matrix and about 15 nm thick amorphous layer near the film-substrate interface. The combination of small grain size and amorphous/nanocrystalline structure can not only inhibit dislocations emission from small nanocrystals, but also prevent emitted dislocations to pass through amorphous/nanocrystalline interface, which limits the plastic energy dissipation in TiN films. A higher degree of film crystallization is observed, with the temperature rise, leading to higher hardness and elastic modulus, but lower fracture toughness of the films after annealing.

Measured adhesion energy gradually increased with annealing temperature, and then dropped at 500 °C. Increasing plastic energy dissipation in the Si substrate induced by thermally activated dislocation glide is argued to be responsible for the enhancement in measured adhesion energy with temperature. The drop in adhesion energy at 500 °C is attributed to local phase transformation from amorphous to nanocrystalline at the interface. Local interfacial crystallization is detrimental for adhesion and has two effects that are acting in cooperation. One is the formation of amorphous/nanocrystalline structure, which contributes to the embrittlement of the interface. The other is that the film crystallization increases the contact misfit of the interface compared with the previous amorphous state. At last, the drop in adhesion also induces circular blisters propagation from axisymmetric to non-axisymmetric.

Acknowledgments

This work was supported by Beijing Nova Program (Z171100001117075), the National Natural Science Foundation of China (51431004).

References

[1] P. Wellner, O. Kraft, G. Dehm, J. Andersons, E. Arzt, Channel cracking of β-NiAl thin films on Si substrates, Acta Mater. 52 (2004) 2325–2336.
[2] L. Hultman, Thermal stability of nitride thin films, Vacuum 57 (2000) 1–30.
[3] R. Vaßen, M.O. Jarligo, T. Steinke, D.E. Mack, D. Stöver, Overview on advanced thermal barrier coatings, Surf. Coat. Technol. 205 (2010) 938–942.
[4] H. Köstenbauer, G.A. Fontalvo, M. Kapp, J. Keckes, C. Mitterer, Annealing of intrinsic stresses in sputtered TiN films: the role of thickness-dependent gradients of point defect density, Surf. Coat. Technol. 201 (2007) 4777–4780.
[5] X.Y. Gong, H. Peng, Y. Ma, H.B. Guo, S.K. Gong, Microstructure evolution of an EB-PVD NiAl coating and its underlying single crystal superalloy substrate, J. Alloy. Compd. 672 (2016) 36–44.
[6] D.R. Mumm, A.G. Evans, On the role of imperfections in the failure of a thermal barrier coating made by electron beam deposition, Acta Mater. 48 (2000) 1815–1827.
[7] A.G. Evans, D.R. Mumm, J.W. Hutchinson, G.H. Meier, F.S. Pettit, Mechanisms controlling the durability of thermal barrier coatings, Prog. Mater. Sci. 46 (2001) 505–553.
[8] K. Xiao, Z.S. Guan, G.J. Wang, L. Jiang, D.B. Zhu, Y.R. Wang, Laser-induced wavy pattern formation in metal thin films, Appl. Phys. Lett. 85 (2004) 1934–1936.
[9] S.J. Yu, X.F. Xiao, M.G. Chen, H. Zhou, J. Chen, P.Z. Si, Z.W. Jiao, Morphological selections and dynamical evolutions of buckling patterns in SiAlNx films: from straight-sided to telephone cord or bubble structures, Acta Mater. 64 (2014) 41–53.
[10] T.R. Hull, J.S. Colligon, A.E. Hill, Measurement of thin film adhesion, Vacuum 37 (1987) 327–330.
[11] D.F. Bahr, J.W. Hoehn, N.R. Moody, W.W. Gerberich, Adhesion and acoustic emission analysis of failures in nitride films with a metal interlayer, Acta Mater. 45 (1997) 5163–5175.
[12] N.R. Mody, R.Q. Hwang, S.V. Taraman, J.E. Angelo, D.P. Norwood, W.W. Gerberich, Adhesion and fracture of tantalum nitride films, Acta Mater. 46 (1998) 585–597.
[13] I. Hofinger, M. Oechsner, H.A. Bahr, M.V. Swain, Modified four-point bending specimen for determining the interface fracture energy for thin, brittle layers, Int. J. Fract. 92 (1998) 213–220.
[14] M. Lane, R.H. Dauskardt, A. Vainchtein, H.J. Gao, Plasticity contributions to interface adhesion in thin-film interconnect structures, J. Mater. Res. 15 (2000) 2758–2769.
[15] M.J. Cordill, D.F. Bahr, N.R. Moody, W.W. Gerberich, Adhesion measurements using telephone cord buckles, Mater. Sci. Eng. A 443 (2007) 150–155.
[16] E. Nikitin, R. Kirchheim, A. Pundt, Determination of adhesion energies by means of hydrogen loading, J. Alloy. Compd. 404 (2005) 477–480.
[17] A. Pundt, E. Nikitin, P. Pekarski, R. Kirchheim, Adhesion energy between metal films and polymers obtained by studying buckling induced by hydrogen, Acta

Mater. 52 (2004) 1579–1587.
[18] M.J. Cordill, N.R. Moody, D.F. Bahr, The effects of plasticity on adhesion of hard films on ductile interlayers, Acta Mater. 53 (2005) 2555–2562.
[19] A.A. Volinsky, N.R. Moody, W.W. Gerberich, Interfacial toughness measurements for thin films on substrates, Acta Mater. 50 (2002) 441–466.
[20] W.W. Gerberich, A.A. Volinsky, N.I. Tymiak, N.R. Moody, A brittle to ductile transition (BDT) in adhered thin films, in: MRS Proceedings, vol. 594, Cambridge Univ Press, 1999, p. p.351.
[21] A.A. Volinsky, N.R. Moody, W.W. Gerberich, Nanoindentation of Au and Pt/Cu thin films at elevated temperatures, J. Mater. Res. 19 (2004) 2650–2657.
[22] T.W. Clyne, S.C. Gill, Residual stresses in thermal spray coatings and their effect on interfacial adhesion: a review of recent work, T. Therm. Spray. Technol. 5 (1996) 401.
[23] M.D. Kriese, N.R. Moody, W.W. Gerberich, Effects of annealing and interlayers on the adhesion energy of copper thin films to SiO 2/Si substrates, Acta Mater. 46 (1998) 6623–6630.
[24] M.J. Cordill, A. Taylor, J. Schalko, G. Dehm, Microstructure and adhesion of as-deposited and annealed Cu/Ti films on polyimide, Int. J. Mater. Res. 102 (2011) 1–6.
[25] S.V. Hainsworth, M.R. McGurk, T.F. Page, The effect of coating cracking on the indentation response of thin hard-coated systems, Surf. Coat. Technol. 102 (1998) 97–107.
[26] N.R. Moody, D.P. Adams, D. Medlin, T. Headley, N. Yang, A.A. Volinsky, Effects of diffusion on interfacial fracture of gold-chromium hybrid microcircuit films, Int. J. Fract. 120 (2003) 407–419.
[27] K. Wu, J.Y. Zhang, G. Liu, P. Zhang, P.M. Cheng, J. Li, G.J. Zhang, J. Sun, Buckling behaviors and adhesion energy of nanostructured Cu/X (X= Nb, Zr) multilayer films on a compliant substrate, Acta Mater. 61 (2013) 7889–7903.
[28] G.D. Sim, J.H. Park, M.D. Uchic, P.A. Shade, S.B. Lee, J.J. Vlassak, An apparatus for performing microtensile tests at elevated temperatures inside a scanning electron microscope, Acta Mater. 61 (2013) 7500–7510.
[29] G.D. Sim, J.J. Vlassak, High-temperature tensile behavior of freestanding Au thin films, Scr. Mater. 75 (2014) 34–37.
[30] Y.B. Xin, K.J. Hsia, Simulation of the brittle-ductile transition in silicon single crystals using dislocation mechanics, Acta Mater. 45 (1997) 1747–1759.
[31] X.Y. Gong, Y. Ma, H.B. Guo, S.K. Gong, Effect of thermal cycling on microstructure evolution and elements diffusion behavior near the interface of Ni/NiAl diffusion couple, J. Alloy. Compd. 642 (2015) 117–123.
[32] P. Bras, J. Sterner, C.P. Björkman, Investigation of blister formation in sputtered Cu2ZnSnS4 absorbers for thin film solar cells, J. Vac. Sci. Technol. A 33 (2015) 061201.
[33] J.W. Hutchinson, M.D. Thouless, E.G. Liniger, Growth and configurational stability of circular, buckling-driven film delaminations, Acta. Metall. Mater. 40 (1992) 295–308.
[34] M.J. Cordill, D.F. Bahr, N.R. Moody, W.W. Gerberich, Recent developments in thin film adhesion measurement, IEEE Trans. Device Mater. Reliab. 4 (2004) 163–168.
[35] N. Matuda, S. Baba, A. Kinbara, Internal stress, Young's modulus and adhesion energy of carbon films on glass substrates, Thin Solid Films 81 (1981) 301–305.
[36] M.J. Cordill, F.D. Fischer, F.G. Rammerstorfer, G. Dehm, Adhesion energies of Cr thin films on polyimide determined from buckling: experiment and model, Acta Mater. 58 (2010) 5520–5531.
[37] A. Pundt, L. Brekerbohm, J. Niehues, P.J. Wilbrandt, E. Nikitin, Adhesion-energy measurements by means of white-light interferometry and controlled-buckling technique, Scr. Mater. 57 (2007) 889–892.
[38] J.W. Hutchinson, Z.G. Suo, Mixed mode cracking in layered materials, Adv. Appl. Mech. 29 (1991) 63–191.
[39] Y. Xiang, T. Li, Z.G. Suo, J.J. Vlassak, High ductility of a metal film adherent on a polymer substrate, Appl. Phys. Lett. 87 (2005) 161910.
[40] A. Lee, B.M. Clemens, W.D. Nix, Stress induced delamination methods for the study of adhesion of Pt thin films to Si, Acta Mater. 52 (2004) 2081–2093.
[41] S.W. Russell, S.A. Rafalski, R.L. Spreitzer, J. Li, M. Moinpour, F. Moghadam, T.L. Alford, Enhanced adhesion of copper to dielectrics via titanium and chromium additions and sacrificial reactions, Thin Solid Films 262 (1995) 154–167.
[42] G.D. Quinn, R.C. Bradt, On the Vickers indentation fracture toughness test, J. Am. Ceram. Soc. 90 (2007) 673–680.
[43] A. Furlan, J. Lu, L. Hultman, U. Jansson, Control of crystallinity in sputtered Cr–Ti–C films, Acta Mater. 61 (2013) 6352–6361.
[44] A. Tarniowy, R. Mania, M. Rekas, The effect of thermal treatment on the structure, optical and electrical properties of amorphous titanium nitride thin films, Thin Solid Films 311 (1997) 93–100.
[45] X.L. Pang, K.W. Gao, H.S. Yang, L.J. Qiao, Y.B. Wang, A.A. Volinsky, Interfacial microstructure of chromium oxide coatings, Adv. Eng. Mater. 9 (2007) 594–599.
[46] L. Tengdelius, M. Samuelsson, J. Jensen, J. Lu, L. Hultman, U. Forsberg, E. Janzén, H. Högberg, Direct current magnetron sputtered ZrB 2 thin films on 4H-SiC (0001) and Si (100), Thin Solid Films 550 (2014) 285–290.
[47] J.M. Gregoire, P.J. McCluskey, D. Dale, S.Y. Ding, J. Schroers, J.J. Vlassak, Combining combinatorial nanocalorimetry and X-ray diffraction techniques to study the effects of composition and quench rate on Au–Cu–Si metallic glasses, Scr. Mater. 66 (2012) 178–181.
[48] G.D. Sim, Y.S. Choi, D. Lee, K.H. Oh, J.J. Vlassak, High tensile strength of sputter-deposited ZrB2 ceramic thin films measured up to 1016 K, Acta Mater. 113 (2016) 32–40.
[49] N. Kumar, M.G. Fissel, K. Pourrezaei, B. Lee, E.C. Douglas, Growth and properties of TiN and TiO x N y diffusion barriers in silicon on sapphire integrated circuits, Thin Solid Films 153 (1987) 287–301.
[50] J.S. Wang, A.G. Evans, Measurement and analysis of buckling and buckle propagation in compressed oxide layers on superalloy substrates, Acta Mater. 46 (1998) 4993–5005.
[51] T. Guo, X.L. Pang, Y.T. Xi, A.A. Volinsky, L.J. Qiao, Externally applied stress sign and film elastic properties effects on brittle film fracture, Philos. Mag. 96 (2016) 447–458.
[52] Q.J. Zhou, J.Y. He, J.X. Li, W.Y. Chu, L.J. Qiao, Measurement of fracture toughness of nickel phosphorus coatings, Mater. Lett. 60 (2006) 349–351.
[53] X.L. Pang, K.W. Gao, F. Luo, H.S. Yang, L.J. Qiao, Y.B. Wang, A.A. Volinsky, Annealing effects on microstructure and mechanical properties of chromium oxide coatings, Thin Solid Films 516 (2008) 4685–4689.
[54] J.J.M. Martınez, A.D. Rodrıguez, F. Monteverde, C. Melandri, G.D. Portu, Characterisation and high temperature mechanical properties of zirconium boride-based materials, J. Eur. Ceram. Soc. 22 (2002) 2543–2549.
[55] F. Ren, E.D. Case, J.E. Ni, E.J. Timm, E.L. Curzio, R.M. Trejo, C.H. Lin, M.G. Kanatzidis, Temperature-dependent elastic moduli of lead telluride-based thermoelectric materials, Philos. Mag. 89 (2009) 143–167.
[56] J.B. Wachtman, D.G. Lam, Young's modulus of various refractory materials as a function of temperature, J. Am. Ceram. Soc. 42 (1959) 254–260.
[57] J.B. Wachtman, W.R. Cannon, M.J. Matthewson, Mechanical Properties of Ceramics, John Wiley & Sons, 2009.
[58] P. Steneteg, O. Hellman, O.Y. Vekilova, N. Shulumba, F. Tasnádi, I.A. Abrikosov, Temperature dependence of TiN elastic constants from ab initio molecular dynamics simulations, Phys. Rev. B 87 (2013) 094114.
[59] H.J. Kim, M.W. Moon, D.I. Kim, K.R. Lee, K.H. Oh, Observation of the failure mechanism for diamond-like carbon film on stainless steel under tensile loading, Scr. Mater. 57 (2007) 1016–1019.
[60] K. Wu, J.Y. Zhang, J. Li, Y.Q. Wang, G. Liu, J. Sun, Length-scale-dependent cracking and buckling behaviors of nanostructured Cu/Cr multilayer films on compliant substrates, Acta Mater. 100 (2015) 344–358.
[61] S. Christiansen, M. Albrecht, H.P. Strunk, S. Veprek, Microstructure of novel superhard nanocrystalline-amorphous composites as analyzed by high resolution transmission electron microscopy, J. Vac. Sci. Technol. B 16 (1998) 19–22.
[62] J. Musil, Hard and superhard nanocomposite coatings, Surf. Coat. Technol. 125 (2000) 322–330.
[63] S. Vepřek, P. Nesladek, A. Niederhofer, F. Glatz, Search for superhard materials: nanocrystalline composites with hardness exceeding 50 GPa, Nanostruct. Mater. 10 (1998) 679–689.
[64] S. Vepřek, S. Reiprich, S.Z. Li, Superhard nanocrystalline composite materials: the TiN/Si3N4 system, Appl. Phys. Lett. 66 (1995) 2640–2642.
[65] G. Wu, K.C. Chan, L.L. Zhu, L.G. Sun, J. Lu, Dual-phase nanostructuring as a route to high-strength magnesium alloys, Nature 545 (2017) 80–83.
[66] J.A. Schneider, S.E. Guthrie, M.D. Kriese, W.M. Clift, N.R. Moody, Effect of carbon on the adhesion of aluminum films to sapphire substrates, in: MRS Proceedings, vol. 522, Cambridge Univ Press, 1998, p. p.347.
[67] S. Timoshenko, Theory of Elastic Stability 2e: Tata McGraw-Hill Education, 1970.
[68] T. Guo, L.J. Qiao, X.L. Pang, A.A. Volinsky, Brittle film-induced cracking of ductile substrates, Acta Mater. 99 (2015) 273–280.
[69] S. Kumar, D.E. Wolfe, M.A. Haque, Dislocation shielding and flaw tolerance in titanium nitride, Int. J. Plast. 27 (2011) 739–747.
[70] V. Lakshmanan, J. Li, Edge dislocations emitted along inclined planes from a mode I crack, Mater. Sci. Eng. A 104 (1988) 95–104.
[71] S.X. Mao, M.Z. Li, Effects of dislocation shielding on interface crack initiation and growth in metal/ceramic layered materials, J. Mech. Phys. Solids 47 (1999) 2351–2379.
[72] S.X. Mao, X.P. Li, Nucleation of nanocracks by a quasicleavage process in a dislocation-free zone, Philos. Mag. A (1999) 1817–1837.
[73] L. Chang, L.C. Zhang, Deformation mechanisms at pop-out in monocrystalline silicon under nanoindentation, Acta Mater. 57 (2009) 2148–2153.
[74] A.M. Minor, E.T. Lilleodden, M. Jin, E.A. Stach, D.C. Chrzan, J.W. Morris, Room temperature dislocation plasticity in silicon, Philos. Mag. 85 (2005) 323–330.
[75] D. Sherman, I. Be'Ery, Dislocations deflect and perturb dynamically propagating cracks, Phys. Rev. Lett. 93 (2004) 265501.
[76] J.R. Rice, R. Thomson, Ductile versus brittle behaviour of crystals, Philos. Mag. 29 (1974) 73–97.
[77] Y.H. Chiao, D.R. Clarke, Direct observation of dislocation emission from crack tips in silicon at high temperatures, Acta Metall. 37 (1989) 203–219.
[78] S. Nakao, T. Ando, M. Shikida, K. Sato, Effect of temperature on fracture toughness in a single-crystal-silicon film and transition in its fracture mode, J. Micromech. Microeng 18 (2007) 015026.
[79] E. Nadgornyi, Dislocation dynamics and mechanical properties of crystals, Prog. Mater. Sci. 31 (1988) 1–530.
[80] M. Tanaka, E. Tarleton, S.G. Roberts, The brittle–ductile transition in single-crystal iron, Acta Mater. 56 (2008) 5123–5129.
[81] A.A. Taylor, M.J. Cordill, L. Bowles, J. Schalko, G. Dehm, An elevated temperature study of a Ti adhesion layer on polyimide, Thin Solid Films 531 (2013) 354–361.